SUPPORTING INFORMATION

MECHANISM OF CALCITE CO-ORIENTATION IN THE SEA URCHIN TOOTH

Christopher E. Killian[1,2], Rebecca A. Metzler[1], Y. U. T. Gong[1], Ian C. Olson[1], Joanna Aizenberg[3], Yael Politi[4], Fred H. Wilt[2], Andreas Scholl[5], Anthony Young[5], Andrew Doran[5], Martin Kunz[5], Nobumichi Tamura[5], Susan N. Coppersmith[1], and

P.U.P.A. Gilbert[1]*

[1]Department of Physics, University of Wisconsin, Madison, WI 53706, USA.

[2]Department of Molecular and Cell Biology, University of California, Berkeley, CA 94720, USA.

[3]School of Engineering and Applied Sciences, Harvard University, Cambridge, MA 02138, USA.

[4]Department of Structural Biology, Weizmann Institute of Science Rehovot 76100, Israel.

[5]Advanced Light Source, Lawrence Berkeley National Laboratory, Berkeley, CA 94720, USA.

* Previously publishing as Gelsomina De Stasio. Corresponding author: pupa@physics.wisc.edu

Figures S1-S8, Methods

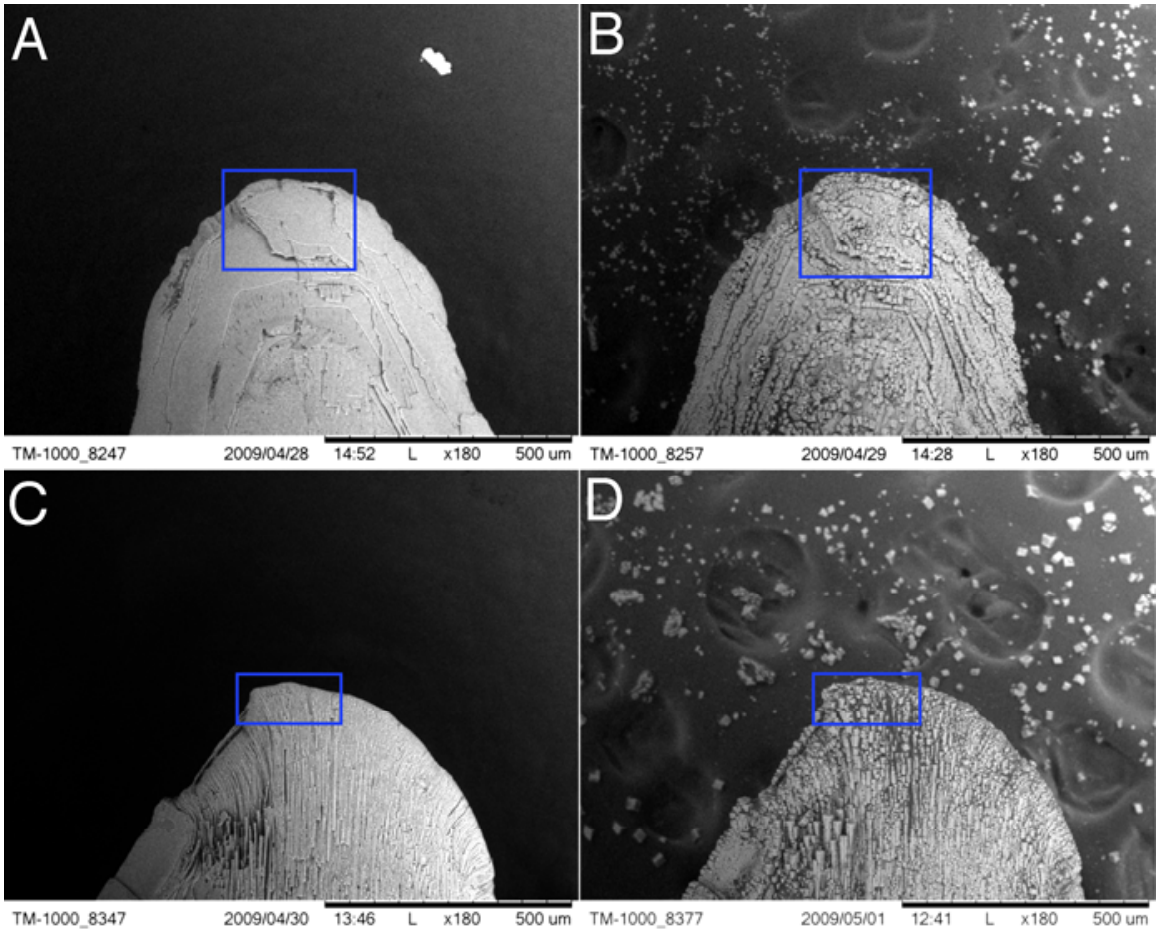

Figure S1. Zoomed-out SEM micrographs of the two sea urchin teeth in Figure 1, and correspondingly labeled A, B, C, D. The boxes indicate the regions magnified in Figure 1.

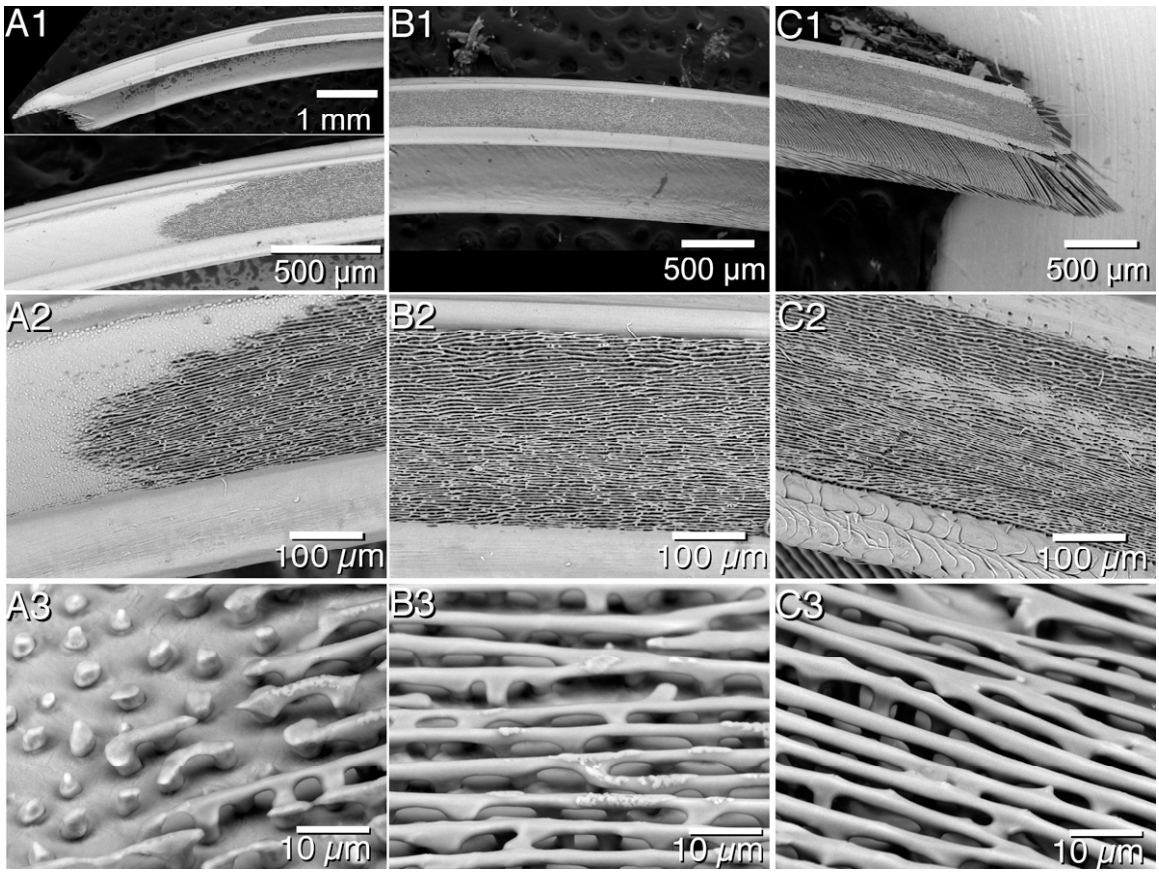

Figure S2. Pillar bridges on the outer surface of a *Strongylocentrotus purpuratus* tooth. (A1-A2-A3) Increasing magnification SEM micrographs at the tip of the tooth, (B1-B2-B3) the middle of the 1.5-cm long tooth, and (C1-C2-C3) the forming end of the tooth, where the polycrystalline matrix has not yet cemented plates and fibers together, and these appear separate and free-standing in space.
Notice that the bridges extend along the entire length of the tooth, but are shed off approximately 3 mm from the tip (A1), and only the footprints of the bridge "piers" remain (A3). Two sets of bridges are present on either side of the tooth. The absence of bridges from the grinding tip of the tooth may explain why they had not been reported in many previous studies. For example in Figure S7 there is no evidence of the bridges, as that cross-section was taken close to the tip. The discovery of these mineral bridges explains how the same crystal orientation is propagated across all plates.

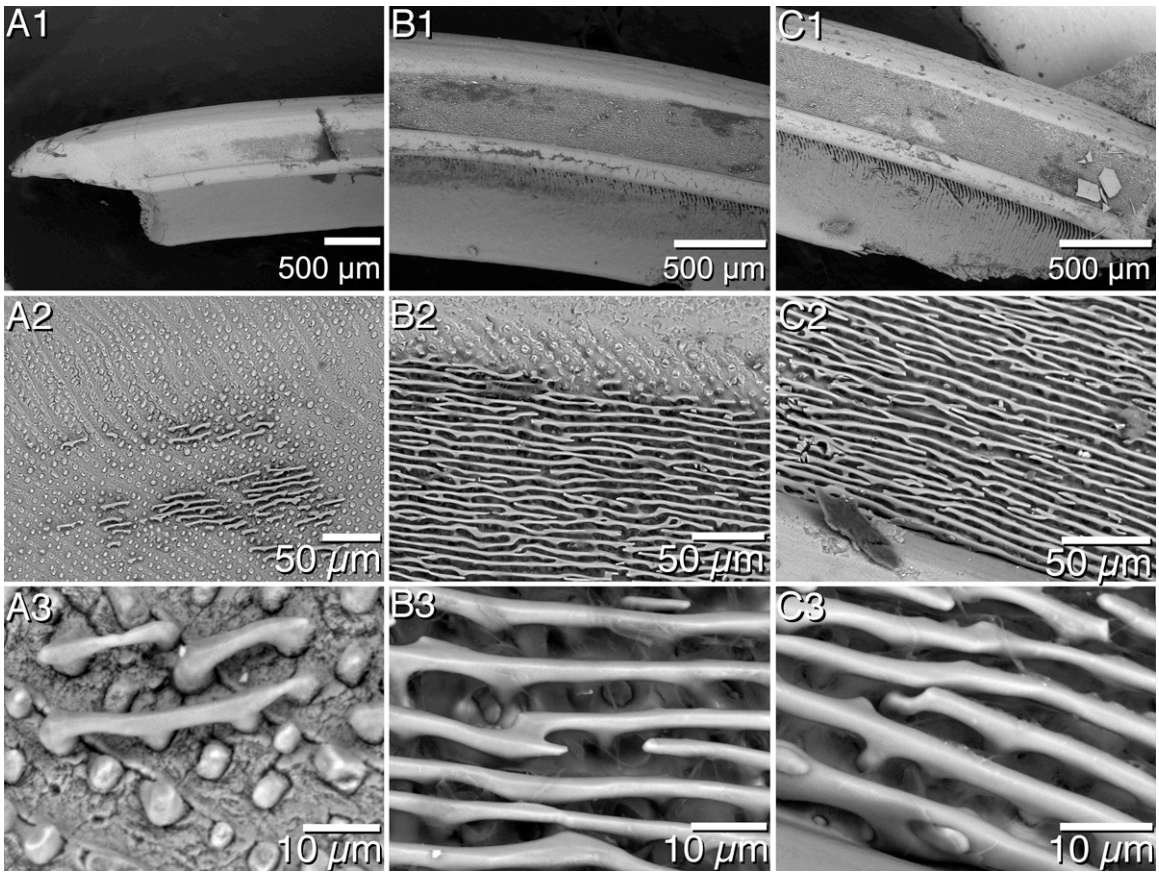

Figure S3. Mineral bridges on a *Paracentrotus lividus* tooth. As in Figure S2, Panels (A1-A2-A3) zoom in on the tooth tip, (B1-B2-B3) the tooth middle, and (C1-C2-C3) the forming end of the tooth. Again the bridges are shed off approximately 2 mm from the grinding tip (A1) and only their footprints remain (A2 and A3).

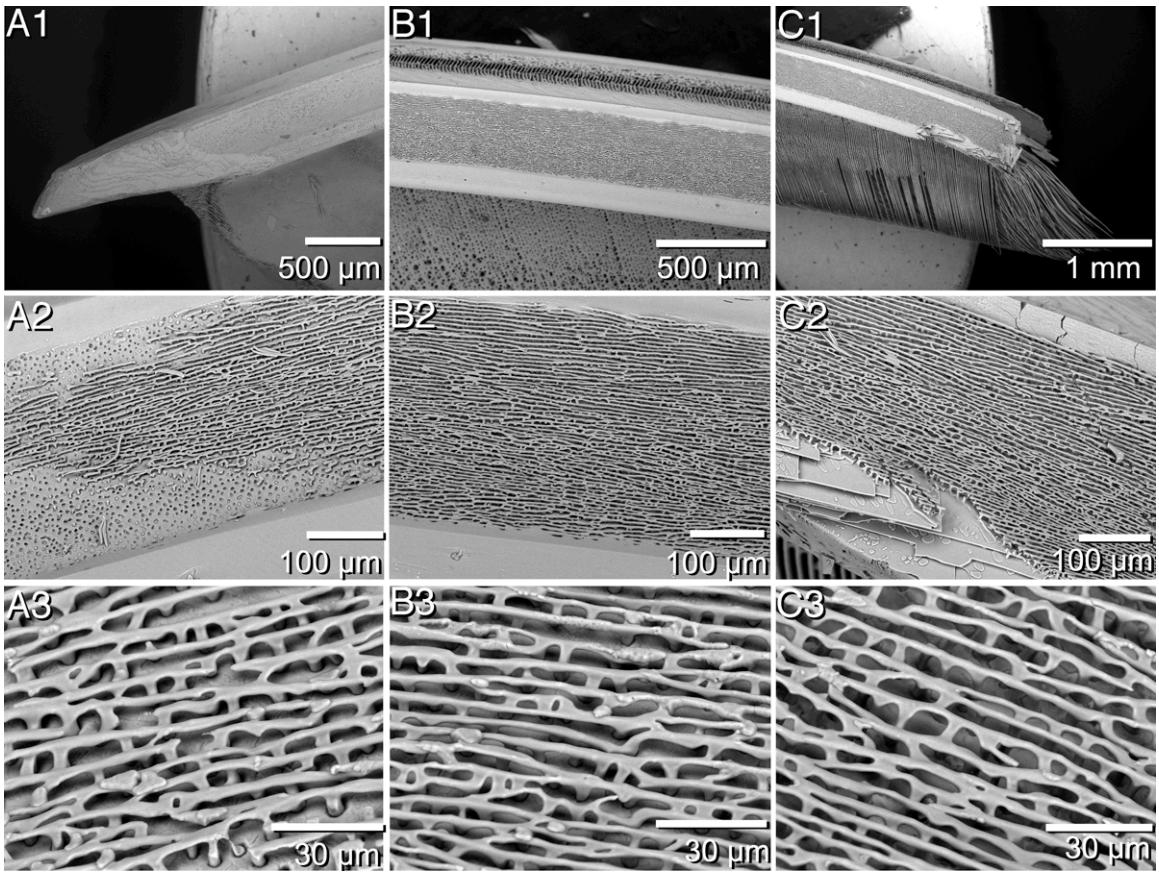

Figure S4. Mineral bridges on a *Lytechinus variegatus* tooth. As in the previous figures, panels (A1-A2-A3) show the tooth tip, (B1-B2-B3) the middle, and (C1-C2-C3) the forming end. Again the bridges are shed off more than 3 mm from the grinding tip, and only their footprints remain (A2).

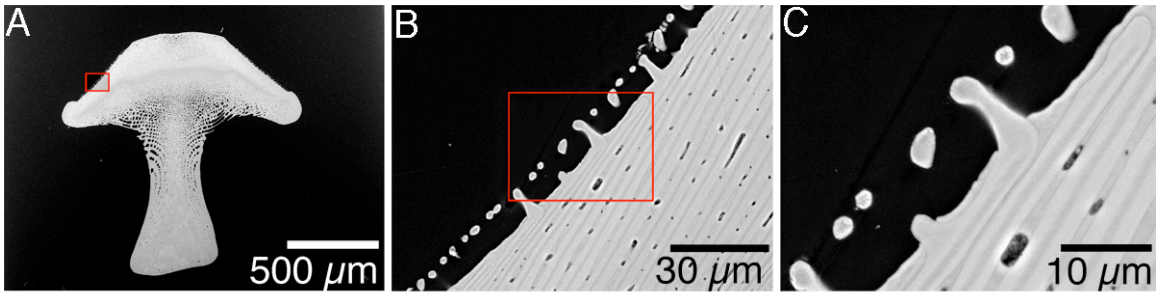

Figure S5. Mineral bridges protruding from the cross-section of a *Paracentrotus lividus* tooth. (A-B-C) Increasing-magnification SEM micrographs of the same sample. The red boxes in A and B indicate the regions magnified in B and C, respectively. In cross-section the bridges clearly protrude from the T-shaped outline of the tooth. The bridge "piers" form 90° angles with the plates, and are continuous with the plates, as clearly seen in C. The bridge "decks" appear as isolated round shapes in cross-section, as they run perpendicular to the plane of the images in B and C. The dark spots in B and C are holes, knows as "cell channels".

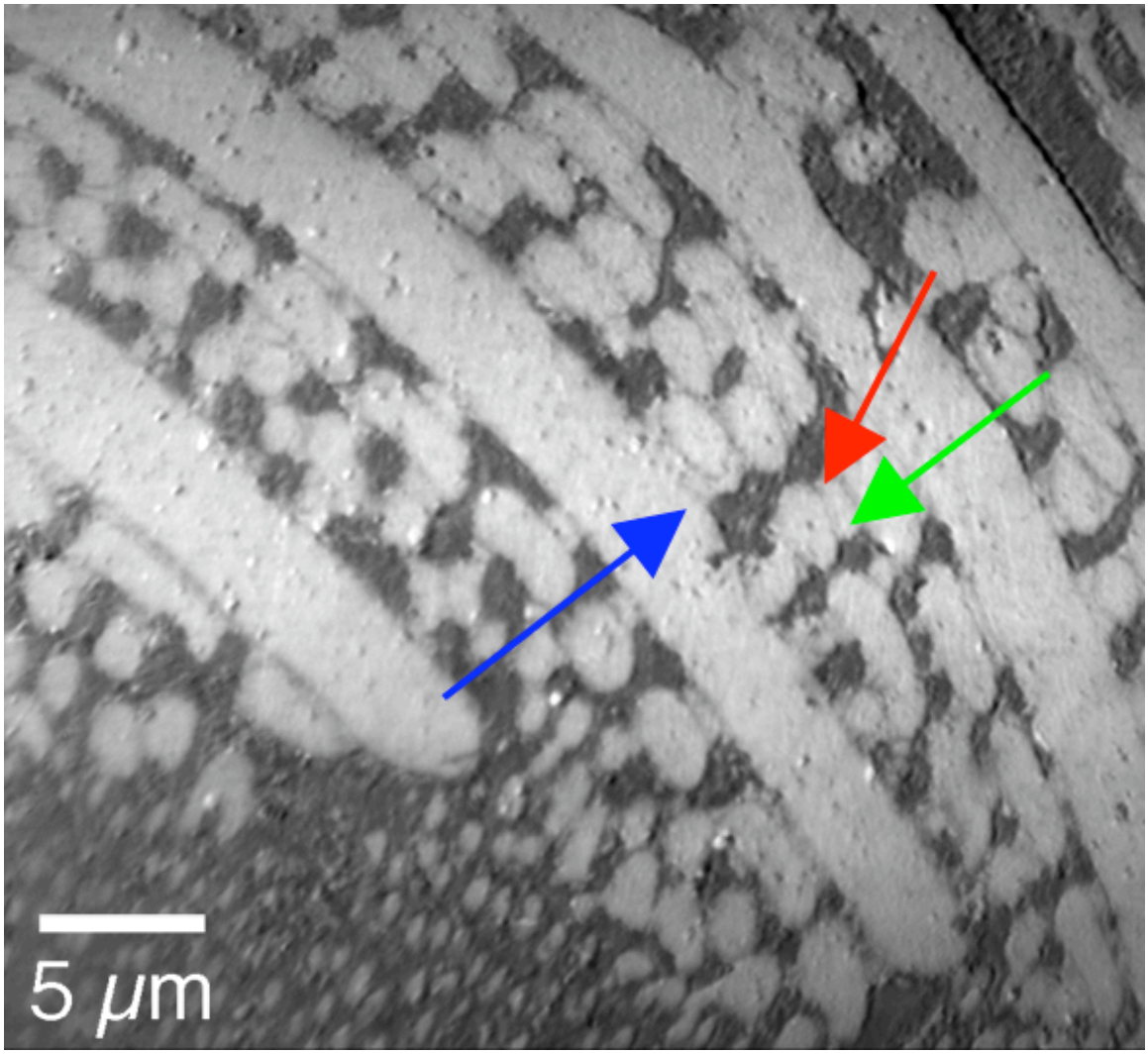

Figure S6. Calcium distribution map, acquired with X-PEEM, of a cross-section of the forming sea urchin tooth. This region was approximately 3 mm away from the forming end of an *S. purpuratus* tooth. Notice that the plates and the fibers are fully formed and mineralized (thus Ca-rich, as indicated by the light gray level), while the matrix between plates and fibers is still forming. The arrows indicate the single pixels (20-nm in size) from which the spectra of Figure 3 were extracted. The amorphous phases occur most frequently in the forming matrix (red and green arrows).

Notice that the Ca-rich regions shown in this cross-section are fully aggregated and *solid*. Individual nanoparticles not yet aggregated, whether amorphous or crystalline, would have been washed away during polishing of this sample, which is done with 50-nm alumina grit in a water suspension (saturated with $CaCO_3$). This is important because it shows that amorphous phases aggregate first (and are observed here), and will be converted into crystals at a later stage.

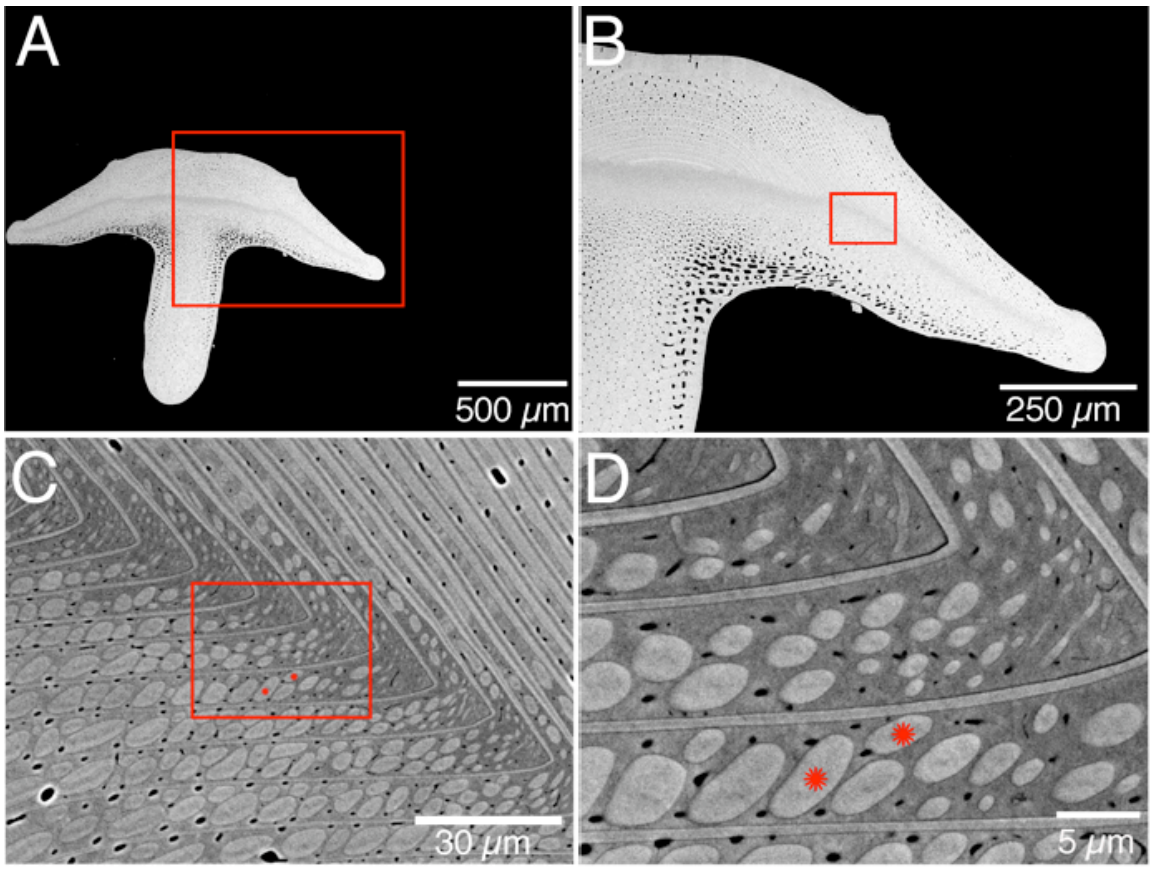

Figure S7. SEM images of the same region in Figure 4. In this region of a sea urchin tooth cross-section, the primary and secondary plates join each other and have a chevron morphology, ~300 micron away from the center of the stone. (A-D) Increasing magnification SEM micrographs of the tooth cross-section. The boxes in A, B and C indicate the areas where the micrographs in B, C, and D were acquired. The asterisks indicate the two fibers with strong mis-orientation in Figure 4.

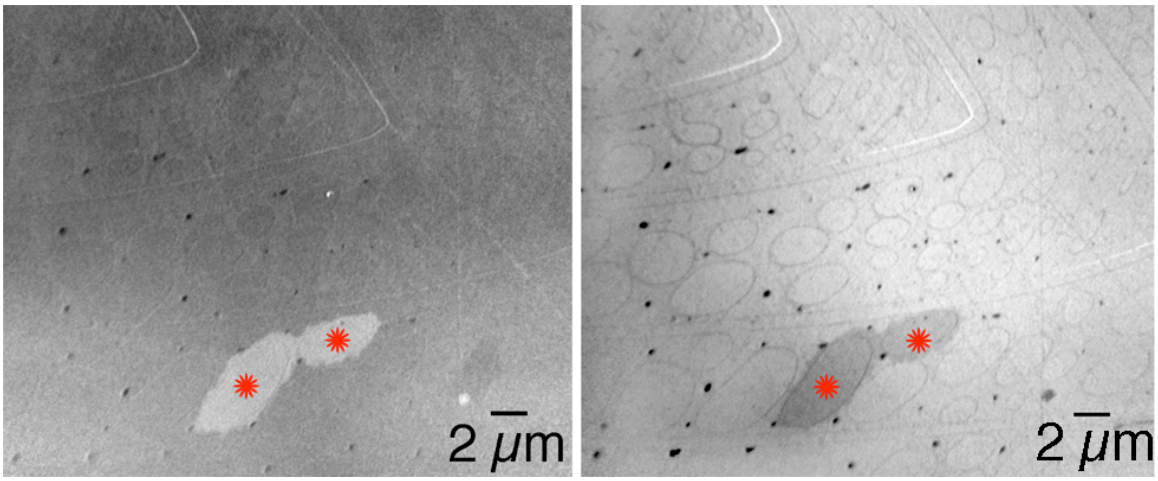

Figure S8. PIC maps of the same region in Figure 4 and S7, acquired with linearly polarized x-ray illumination with horizontal (0°, left) and vertical polarization (90°, right). (Figure 4A was acquired with a polarization angle of 45°.) Notice that at these polarization angles the plates, the fibers and the polycrystalline matrix all exhibit similar gray levels, while the two stray fibers (asterisks) are strongly different. This means that the crystal orientation difference between the plates and the surrounding matrix observed in the PIC maps of Figure 4A and Figure 5 is small (3°-4°, as observed by μXRD), while the mis-orientation of the stray fibers is large (~14°, again from μXRD).

The crystal orientation of the stray fibers spills out of the fibers into the surrounding polycrystalline matrix nanoparticles.

A very technical observation, which a general audience should neglect, is that there is a gradient of contrast across the image in Figure 4A: higher contrast on top, lower at the bottom. This is due to the combined effects of energy dispersion across the image and the narrowness of the π* peak we are imaging in a PIC map. The contrast is higher at the top of the image and lower at the bottom, thus the plates appear with a different gray level with respect to the surrounding matrix, while the bottom plates exhibits almost no contrast. It is remarkable, however, that the stray fibers appear in the low-contrast region and still exhibit strong contrast. This also confirms that they are strongly mis-oriented with respect to all other features in the image.

METHODS

Samples

Specimens of *Strongylocentrotus purpuratus* were collected from the intertidal zone near Bodega Bay, California, and kept in 15°C seawater aquaria for a few months. *S. purpuratus* teeth were extracted from freshly sacrificed sea urchins. The teeth were manually separated from the Aristotle's lantern and from the plumula. The teeth were fixed for 30 minutes in 4% paraformaldehyde in seawater that had been saturated with $CaCO_3$ and filtered. The fixed teeth were then rinsed twice in $CaCO_3$-saturated water, twice in $CaCO_3$-saturated ethanol and air-dried. $CaCO_3$-saturation was used to avoid dissolving ACC phases, which are much more soluble than crystalline calcite. The dry teeth were then embedded into epoxy resin (Epoxicure resin and hardener, Buehler, Lake Bluff, IL). Once cured overnight, the blocks were polished with decreasing size alumina grit down to 0.05 μm (Masterprep, Buehler, Lake Bluff, IL) so that their growth direction was either in-plane in longitudinal sections, or normal in cross-sections. Finally the samples were sputter coated with 1-nm Pt in the area to be analyzed by X-PEEM, and 40 nm Pt around it, to provide electrical conductivity to the otherwise insulating crystals[1]. Fresh teeth to be analyzed for ACC were kept on dry ice at all times, except when epoxy-curing overnight, polishing and Pt-coating. During these procedures, however, they were kept away from air to prevent ACC crystallization, which occurs upon contact with water or air moisture. During epoxy-curing, the samples were kept in a desiccator, during coating in low vacuum, and during transfers and mountings they were handled rapidly, using gloves and face masks.

Teeth for SEM analysis in Figures 1 and S1 were not fixed. They were bleached to remove the surface organics and expose the clean mineral surfaces. SEM analysis of bleached samples reveals identical morphology as for fixed teeth, the only difference is that they appear cleaner. The mechanical hardness and toughness of bleached samples, however, was much inferior to unbleached samples.

SEM analysis was done at the Electron Microscopy Lab, University of California at Berkeley. The environmental SEM used is a Hitachi TM1000 SEM, in the back-scattered electron (BSE) imaging mode. This environmental SEM does not require sample coating, which was crucial to observe the exact same tooth locations before and after calcite crystal overgrowth.

Samples for μXRD included: the same embedded, polished and coated samples analyzed with X-PEEM, in which the same regions were identified by optical microscopy, and μXRD was done in reflection mode; Other samples were entire sea urchin teeth separated from the Aristotle's lantern, bleached, rinsed in ethanol, and air dried. Only the tip of these teeth was analyzed in the transmission mode, and yielded the best data from matrix only, or a single plate tip overlapping the matrix in the beam path. Other teeth, also analyzed in transmission mode, were tripod-polished to form a wedge of varying thickness, at a 2° angle. The resulting thinnest

portion of the teeth was estimated to be on the order of 100-200 nm. These samples yielded terraced plates, so that 1, 2, 3, or 4 plates were in the beam path at once, with sharp separations easily detectable by x-ray fluorescence.

Calcite Overgrowth

Bleached teeth were mounted on SEM stubs with carbon tape. After control SEM images of the samples were taken, the mounted teeth were placed in a Costar 12-well polystyrene culture dish and immersed in 10 mM $CaCl_2$. The wells were covered with aluminum-foil and the foil was sealed at its edges with parafilm. Three small holes were opened in the foil with a needle. The culture dish with the sample teeth was placed in a desiccator containing two uncovered 80 ml beakers of ammonium carbonate. The desiccator was sealed and evacuated using the house vacuum. After incubating at room temperature for 16 hours, the samples were removed, rinsed with $CaCO_3$-saturated ethanol, and air-dried. SEM images of the decorated teeth were then taken.

X-PEEM and XANES

X-PEEM and XANES spectra on the sea urchin teeth were acquired using the PEEM-3 microscope at the Advanced Light Source. Briefly, the sample is mounted vertically and the x-ray beam illuminates the sample at a grazing incidence angle of 30°, while the optics column is horizontal, and along the normal to the sample surface. The x-ray beamline energy range is 200-2000 eV, and a Ti-filter was used to minimize second-order transmission. All Ca L-edge spectra were normalized to a linear background, and then aligned in energy and intensity so that the Ca L_2 peak is at 352.6 eV, and its intensity is 1. The spectra were then displaced vertically for clarity. Ca and Mg maps were obtained by digital ratio of two images acquired on- and off-peak, at the Ca L-edge (352.6 eV and 342 eV) and the Mg K-edge (1315 eV and 1309 eV).

The straight lines seen in all X-PEEM images are scratches produced during polishing on the surface of the sea urchin tooth.

PIC images

Polarization-dependent imaging contrast (PIC) maps were obtained by ratio of two images acquired at the anti-correlated π^* and σ^* peak energies, 290.3 and 302 eV, respectively. Both peaks and their anti-correlation are characteristic of carbonate groups, and they are distinct in calcite and aragonite[2,3]. The source for the PEEM-3 x-ray beamline is an elliptically polarizing undulator (EPU)[4,5], in which the linear polarization can be rotated by 90°. In this work this feature was used extensively to yield the highest possible contrast for each image.

Quantitative analysis of c-axis orientation in PIC maps is hindered by the gradient of x-ray intensity across the field of view described in Figure 5. A semi-quantitative estimate, however, is made possible by the observation that small c-axis angle differences (measured by diffraction[3]), on the order of a few degrees, are usually only observed at specific polarization angles and not others. This is the case of the plates in the sea urchin tooth, whose gray level in a PIC map is slightly different

from that of the surrounding matrix and fibers at a 45° polarization angle, but not at 0 or 90° angles (compare the plates' contrast in Figure 4A and S6). Ma et al. did not notice the small plates' contrast in *P. lividus* as the alternating co-oriented blocks (which are not present in *S. purpuratus*), with c-axes 6° or less apart from each other, exhibited much greater contrast[6]. The plates' orientation in *P. lividus*, therefore, must be much smaller than 6°, on the order of 1° or 2° different from the surrounding fibers and matrix. This is consistent with the present semi-quantitative observation in *S. purpuratus*. When c-axis angle differences are much larger, their contrast is visible at a variety of polarization angles. This is the case of the stray fibers in Figures 4A and S6, exhibiting strong contrast at 0°, 45° and 90° polarizations, thus the angle between the stray fibers' c-axis and that of the distant mineral components must be on the order of tens of degrees.

The calcite crystal overgrowth experiments of Figure 1B show that all plates are co-oriented with respect to each other, and this is consistent with the gray levels in the PIC map of Figure 5, which are similar across the plates but distinct from the gray levels for the rest of the tooth components. Fibers and polycrystalline matrix in the stone part are closely co-oriented, as shown at the bottom of Figure 5. The stone part of the tooth is continuous with the distal tip. Therefore these observations are consistent with the overgrowth experiments of Figure 1D.

Image manipulation

Image manipulation was kept to a minimum. For all X-PEEM and SEM images only the contrast was adjusted, using Adobe Photoshop® for MacIntosh, and this was done to the entire image. In Figure 5 the contrast was adjusted for all images at once (in each of the three panels), after overlapping them while they were temporarily made semi-transparent. Boxes, arrows, letters and asterisks were added in Adobe Photoshop® on separate layers, and the original images are available upon request.

The only processing not applied to entire images is the addition of color in Figure 1. In this case the entire image was converted to a tritone (magenta or green), then the mis-oriented rhombohedra were cut out, to reveal an underlying layer in which a different tritone (blue) was used for the same image. The edges of the rhombohedra are sharp and well defined, thus the choice of where to cut was never done arbitrarily or subjectively. The co-orientation of magenta and green rhombohedra was carefully measured with a reference frame of axes moved from one rhombohedron to the next. The accuracy of this measurement is estimated to be better than 0.5°, when the images are magnified on a large monitor, as was done for Figure 1.

μXRD

S. purpuratus teeth were analyzed either in transmission or in reflection mode, using 1 μm x 1 μm pink beam of photon energy 5-22 keV, from a super-bend source at the Advanced Light Source, beamline 12.3.2[7,8]. In the reflection mode the horizontal μ-beam illuminated the sample, mounted at 45°, and the X-Ray CCD detector (MAR133 from MAR, now Rayonix) was vertical and on top, with the active area at 89 mm

distance from the sample, while in the transmission mode the detector was rotated to be co-axial with the beam, and the sample was mounted vertically. The sample was mounted on and x-y-z scanning stage, so either maps or single (Laue) XRD patterns could be acquired. Fluorescence maps were always acquired first using a solid state detector (Vortex, SII Technologies), to identify specific regions of interest, and image them at the Ca K-edge, then Laue μXRD patterns were collected with exposure times varying between 1 sec and 5 sec, and processed using XMAS (X-ray Microdiffraction Analysis Software), developed by one of us (N.T.).

REFERENCES

(1) De Stasio, G.; Frazer, B. H.; Gilbert, B.; Richter, K. L.; Valley, J. W. *Ultramicroscopy* **2003**, *98*, 57-62.

(2) Metzler, R. A.; Zhou, D.; Abrecht, M.; Chiou, J.-W.; Guo, J.; Ariosa, D.; Coppersmith, S. N.; Gilbert, P. U. P. A. *Physical Review B* **2008**, *77*, 064110-1/9.

(3) Gilbert, P. U. P. A.; Metzler, R. A.; Zhou, D.; Scholl, A.; Doran, A.; Young, A.; Kunz, M.; Tamura, N.; Coppersmith, S. N. *J. Am. Chem. Soc.* **2008**, *130*, 17519-17527.

(4) Carr, R.; Kortright, J. B.; Rice, M.; Lidia, S. *Rev Sci Instrum* **1995**, *66*, 1862.

(5) Young, A. T.; Feng, J.; Arenholz, E.; Padmore, H. A.; Henderson, T.; Marks, S.; Hoyer, E.; Schlueter, R.; Kortright, J. B.; Martynov, V.; Steier, C.; Portmann, G. *Nucl Instrum & Meth A* **2001**, *467-468*, 549-552.

(6) Ma, Y. R.; Aichmayer, B.; Paris, O.; Fratzl, P.; Meibom, A.; Metzler, R. A.; Politi, Y.; Addadi, L.; Gilbert, P. U. P. A.; Weiner, S. *Procs. Natl. Acad. Sci. USA* **2009**, *106*, 6048-6053.

(7) Tamura, N.; MacDowell, A. A.; Spolenak, R.; Valek, B. C.; Bravman, J. C.; Brown, W. L.; Celestre, R. S.; Padmore, H. A.; Batterman, B. W.; Patel, J. R. *J Synchr Radiat* **2003**, *10*, 137-143.

(8) Kunz, M.; Tamura, N.; Chen, K.; MacDowell, A. A.; Celestre, R. S.; Church, M. M.; Fakra, S.; Domning, E. E.; Glossinger, J. M.; Kirschman, J. L.; Morrison, G. Y.; Plate, D. W.; Smith, B. V.; Warwick, T.; Yashchuk, V. V.; Padmore, H. A.; Ustundag, E. *Rev Sci Instrum* **2009**, *80*, 03510.